Available online at www.sciencedirect.com
SCIENCE DIRECT®
Journal of Chromatography A, 983 (2003) 51–71
JOURNAL OF CHROMATOGRAPHY A
www.elsevier.com/locate/chroma

Study of the mass transfer kinetics in a monolithic column

F. Gritti[a,b], W. Piatkowski[a,b,1], G. Guiochon[a,b,*]

[a]*Department of Chemistry, University of Tennessee, 552 Buehler Hall, Knoxville, TN 37996-1600, USA*
[b]*Division of Chemical and Analytical Sciences, Oak Ridge National Laboratory, Oak Ridge, TN, USA*

Received 2 August 2002; received in revised form 1 October 2002; accepted 1 October 2002

Abstract

The purpose of this work is to investigate the mass transfer kinetics of butylbenzoate on a monolithic RPLC column, with methanol–water (65:35, v/v) as the mobile phase. We used the perturbation method, measuring the height equivalent to a theoretical plate (HETP) of the peaks obtained as the response to small pulses of solute injected on a concentration plateau. The equilibrium isotherm of butylbenzoate was previously determined by frontal analysis. It is well accounted for by a liquid–solid extended multilayer BET isotherm model. The equilibrium data derived from the pulse method are in excellent agreement with those of frontal analysis in the accessible concentration range of 0 to 8 g/dm^3. Plots of the HETP of small pulses, injected on eight different plateau concentrations, were acquired in a wide range of mobile phase flow velocities. The axial dispersion and the mass transfer kinetic coefficients were derived from these data. The validity of these measurements is discussed. The mass kinetics of butylbenzoate depends strongly on the plateau concentration. Processes involving adsorptive interactions between the solute and the stationary phase, e.g. surface diffusion and adsorption–desorption kinetics, combine in series to the external mass transfer kinetics and to effective pore diffusivity.

Keywords: Mass transfer; Kinetic studies; Monolithic columns; Adsorption isotherms; Perturbation chromatography; Frontal analysis; BET model; Column efficiency; Axial dispersion; Mathematical modeling

1. Introduction

With the aim of increasing column efficiencies and/or reducing analysis times, efforts were made in the 1970s to reduce the average size of the particles of conventional spherical packing materials [1–3]. Because any reduction in the particle size leads to a strong increase in the required head pressure, this trend has abated for the last 20 years. The most efficient columns that can be used in current practice are 25 cm long and are packed with 3 μm particles. Further progress can come only from a novel approach. The recent advent of commercially available monolithic columns [4–9], offers new practical possibilities for decreasing retention times and/or increasing column efficiencies while escaping the pressure constraint to a certain extent. The topical manufacturing of these monolithic columns is based on a sol–gel process [4] which results in a single piece of solid silica adsorbent that possesses an interconnected skeleton and interconnected flow paths through this skeleton. Tanaka and co-workers

*Corresponding author. Tel.: +1-865-974-0733; fax: +1-865-974-2667.
E-mail address: guiochon@utk.edu (G. Guiochon).
[1]On leave from the Faculty of Chemistry, Rzeszów University of Technology, W. Pola 2 Street, 35-959 Rzeszów, Poland.

0021-9673/02/$ – see front matter
PII: S0021-9673(02)01648-5

[5–7] showed that the size distributions of the flow paths and of the silica skeleton can be controlled independently, a critical property because the former control the bed porosity and permeability like the interstitial volumes in packed columns, while the size of the latter controls the mass transfer kinetics, hence the column efficiency like the diameter of the particles in packed beds. So, when large through-pores are combined with a network of fine silica rods, a monolith exhibits a high external porosity, hence a high total porosity (0.80–0.90 instead of 0.50–0.7 for packed columns) and a low hydraulic resistance and it has a low height equivalent to a theoretical plate (HETP) at high flow-rates, due to the decreased diffusion path length through the skeleton [10–13]. Finally, the average size of the mesopores in the skeleton, hence the surface area available for solute adsorption and retention, can be adjusted by treating the gel with proper aqueous solutions of ammonium hydroxide. The limiting step in the fabrication of silica monoliths stems from the slow rate at which the gel must be dried. When cylindrical monoliths are dried too fast, they exhibit radial heterogeneity, resulting in a low column efficiency and a fragile silica rod. Consequently, the preparation of monoliths wider than a few millimetres is difficult and long. Only analytical columns are now commercially available. Everything else being constant, the time that it takes to dry a monolith is proportional to the square of its diameter which leaves little hope for the early availability of preparative size monoliths.

The reproducibility of the retention data and band profiles obtained on monolithic columns were studied by Kele and Guiochon [14] on a series of six Chromolith Performance RP-18e columns (Merck, Darmstadt, Germany). Made of a C_{18} chemically bonded silica and belonging to six different production batches, these columns exhibited a high degree of reproducibility. They also had a high efficiency. Recently, we showed that the adsorption capacity of these monolithic columns was ~1.4 higher than that of a comparable packed column, in spite of the close values of the surface areas of silica in both columns [15,16]. Hence, the combination of a high permeability and a large adsorption capacity makes monolithic columns very attractive tools for high-speed chromatography, especially for the separation of biological macromolecules [17–23].

The goal of this work is to investigate the mass transfer kinetics of butylbenzoate which has provided unusual and unexpected results in a prior comparative investigation of the thermodynamics of non-linear equilibrium on conventional and monolithic columns [15]. The breakthrough curves obtained in frontal analysis have a front shock layer at low concentrations and a diffuse boundary layer at high concentrations. The converse profile is observed for the desorption curves. This suggests an unusual kinetics of mass transfer, depending strongly on the concentration. To acquire relevant kinetics data, we measured the HETP of small butylbenzoate peaks obtained by injecting small pulses on concentration plateaus of butylbenzoate, in a wide range of the methanol–water mobile phase velocity. The retention times and widths at half-height of these positive or negative perturbation peaks were determined. This pulse method was validated by comparing the adsorption isotherm data obtained by this method and those measured by frontal analysis [15].

2. Theory

2.1. Determination of single-component isotherms by frontal analysis method

Among the various chromatographic methods available to determine single-component isotherms, frontal analysis (FA) is the most accurate [24,25]. It consists in quickly replacing, in step-wise fashion, the stream of mobile phase percolating through the column with solutions of the studied compound of increasing concentrations and in recording the breakthrough curves at the column outlet. Mass conservation of the solute between the times when the new solution enters the column and when the plateau concentration is reached ($A_1+A_2+A_3+A_4$=total mass injected) allows the calculation of the adsorbed amount, q^*, of solute in the stationary phase at equilibrium with a given concentration, C, in the mobile phase. Area A_2 in Fig. 1 represents this amount. This area is best measured by integrating the breakthrough curve (equal area method) [26]. The area on the left of the breakthrough curve ($A_1 + A_2$) is the mass of solute constantly present in the column, i.e. the sum of the mass of solute in the mobile phase occupying the column void-volume

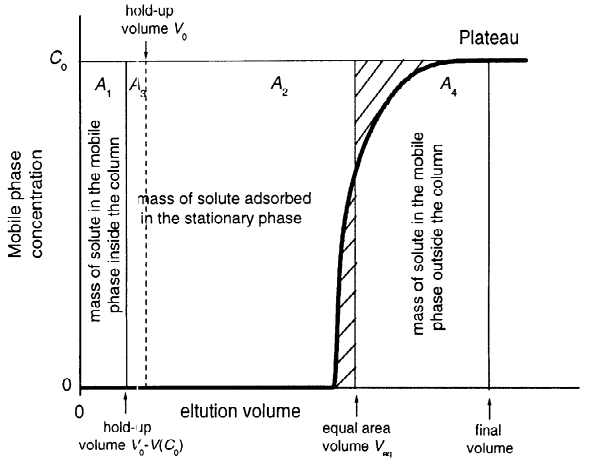

Fig. 1. Frontal analysis method of determination of the equilibrium concentrations in the stationary phase. The breakthrough curve is represented by the thick solid line. The two-hatched surfaces on the right and left side of the breakthrough curve have the same area and fix the volume of equivalent area used for the calculation. A large error may be made if the inflection point is considered. The error made in the determination of the amount adsorbed resulting from an incorrect estimate of the area A_3 is neglected.

(A_1) and the mass of solute adsorbed in the stationary phase (A_2). The adsorbed amount q^* is given by:

$$q^* = \frac{C(V_{eq} - V_0)}{V_a} \tag{1}$$

where V_{eq} and V_0 are the elution volume of the equivalent area and the hold-up volume, respectively, and V_a is the volume of stationary phase. This equation is valid if the hold-up volume remains constant, whatever the equilibrium concentration C in the mobile phase. This condition is generally fulfilled for monolayer adsorption isotherms, for which the volume occupied by the adsorbed monolayer is negligible compared to the void volume. Conversely, in the case of multilayer adsorption isotherms, the pore volume, hence the total porosity, decreases with decreasing volume of pores, $V(C)$, that is occupied by the increasing amount of the adsorbed solute molecules. The area A_3 represents the error of mass (negative) that is made when the variation of the mesopore volume is neglected. The adsorbed amount q^* should be corrected as follows:

$$q^* = \frac{C(V_{eq} - V_0 + V(C))}{V_a} \tag{2}$$

$V(C)$ can be measured by recording the retention time of a non-retained compound at the plateau concentration, C. It is assumed that the volume of stationary phase, V_a, needed to calculate the amount adsorbed per unit volume (i.e. the volume of the C_{18} bonded silica) is independent of the mobile phase concentration.

2.2. Determination of single-component isotherms by perturbation chromatography method

Perturbation chromatography or the pulse method may also be used to measure adsorption isotherm data. We used the method of elution on a plateau, first suggested by Reilley et al. [27]. In this method, small amounts of the sample are injected into the column, first pre-equilibrated at the given plateau concentration. Assuming the ideal model of chromatography, the mass balance equation of a single component can be expressed by the following partial differential equation:

$$\frac{\partial C}{\partial t} + \frac{1 - \varepsilon_t^0}{\varepsilon_t(\bar{C})} \cdot \frac{\partial q}{\partial t} + u \cdot \frac{\partial C}{\partial z} = 0$$
$$\text{with } u = \frac{\dot{V}L}{\varepsilon_t(\bar{C})V_{col}} \tag{3}$$

Eq. (3) assumes that the total porosity, $\varepsilon_t(\bar{C})$, depends on the plateau concentration, $\bar{C}$. ε_t^0 is the total porosity when the column is equilibrated with the pure mobile phase (i.e. for a plateau concentration equal to zero). q and C are the concentrations of the solute at time t and location z, in the stationary and the mobile phase, respectively. u is the linear velocity related to the flow-rate $\dot{V}$, the total porosity, and the column cross-section area. Eq. (3) can be rewritten using the derivative of the composition function $q(C(t))$ and the hypothesis of the local disturbance (q is a linear function of C around $\bar{C}$):

$$\frac{\partial C}{\partial t} + u_z(\bar{C}) \cdot \frac{\partial C}{\partial z} = 0$$
$$\text{with } u_z(\bar{C}) = \frac{u}{1 + \dfrac{1 - \varepsilon_t^0}{\varepsilon_t(\bar{C})} \cdot \left.\dfrac{dq}{dC}\right|_{\bar{C}}} \tag{4}$$

The principle of the perturbation method assumes that an infinitely small perturbation of the equilibrium system is made. Hence, the derivative dq/dC

remains constant and equal to the slope of the adsorption isotherm at the plateau concentration $\overline{C}$. Eq. (4) is the classical propagation equation of the concentration $\overline{C}$. The perturbation peak should thus move at the velocity $u_z(\overline{C})$ and be detected at the outlet of the column at the time:

$$t_R(\overline{C}) = \frac{\varepsilon_t(\overline{C})V_{col}}{\dot{V}} \cdot \left(1 + \frac{1-\varepsilon_t^0}{\varepsilon_t(\overline{C})} \cdot \frac{dq}{dC}\bigg|_{\overline{C}}\right) \quad (5)$$

Eq. (5) allows the determination of the local slope of the adsorption isotherm. This is the thermodynamic information provided by the perturbation method.

2.3. Determination of the local efficiency given by the perturbation method

Due to molecular and eddy diffusion and to the mass transfer resistances, an actual chromatographic system is never ideal. These effects are lumped into the local efficiency at the plateau concentration $\overline{C}$. Since the perturbation theory assumes the isotherm to be locally linear, the pulse peaks should have a Gaussian profile, if we assume that the effect of the various kinetic phenomena is equivalent to those of a random-walk model [28]. To eliminate small non-linear effects, negative ($\overline{C}_-$) and positive ($\overline{C}_+$) pulses are recorded at the plateau concentration $\overline{C}$. The local efficiency is taken as the average, given by:

$$N(\overline{C}) = 5.545\left(\frac{t_R(\overline{C}_+) + t_R(\overline{C}_-)}{\omega_{1/2}(\overline{C}_+) + \omega_{1/2}(\overline{C}_-)}\right)^2 \quad (6)$$

and HETP $= L/N$

where $\omega_{1/2}(\overline{C}_-)$ and $\omega_{1/2}(\overline{C}_+)$ are the widths at half-height of the negative and the positive perturbation peaks, respectively. $t_R(\overline{C}_-)$ and $t_R(\overline{C}_+)$ are the corresponding retention times. They should be equal to the elution time $t_R(\overline{C})$ if the negative and the positive perturbations are small enough.

2.4. Model of isotherm: the liquid–solid extended BET isotherm

The adsorption isotherm equation that best describes the adsorption isotherm data of butylbenzoate on the column used here is the extended Brunauer, Emmett, and Teller (BET) model, widely applied in gas–solid equilibria. This model assumes multilayer adsorption [29]. It was developed to describe adsorption phenomena in which successive molecular layers of adsorbate form at pressures well below the pressure required for completion of the monolayer. The form of this model extended to liquid–solid chromatography was derived and detailed in Ref. [15]. It has the following final expression:

$$q^* = q_S \cdot \frac{b_S C}{(1 - b_L C)(1 - b_L C + b_S \overline{C})} \quad (7)$$

In this model, q_S is the monolayer saturation capacity of the adsorbent, b_S is the equilibrium constant for surface adsorption–desorption (over the free surface of the adsorbent) and b_L is the equilibrium constant for surface adsorption–desorption over a layer of adsorbate molecules.

2.5. Modeling of high-performance liquid chromatography

The profiles of the frontal analysis breakthrough curves and of the perturbation peaks were calculated using the equilibrium-dispersive (ED) model of chromatography [24,25,30]. This model assumes instantaneous equilibrium between the mobile and the stationary phases but a finite column efficiency. The latter is assumed to originate from an apparent axial dispersion coefficient, D_a, accounting for all the dispersive phenomena (molecular, eddy, flow diffusions and non-equilibrium effects as well) that take place in the column.

$$D_a = \frac{uL}{2N} \quad (8)$$

where u is the mobile phase linear velocity, L the column length, and N the number of theoretical plates or apparent efficiency of the column.

In this model, the mass balance equation for a single component is expressed as follows:

$$\frac{\partial C}{\partial t} + u \cdot \frac{\partial C}{\partial z} + F \cdot \frac{\partial q^*}{\partial t} - D_a \cdot \frac{\partial^2 C}{\partial z^2} = 0 \quad (9)$$

where q^* and C are the stationary and mobile phase concentrations of the adsorbate, respectively, t is the time, z the distance along the column and $F = (1 - \varepsilon_t^0)/\varepsilon_t(\overline{C})$ the phase ratio at the plateau concentration

$\overline{C}$. q^* is related to C through the isotherm equation, $q^* = f(C)$.

2.5.1. Initial and boundary conditions for ED model

At $t = 0$ the concentration of the adsorbate in the column is uniformly equal to zero and the stationary phase is in equilibrium with the pure mobile phase. The boundary conditions used are the classical Dankwerts-type boundary conditions [31] at the inlet and outlet of the column.

2.5.2. Numerical solutions of the ED model

The ED model was solved using a computer program based on an implementation of the method of orthogonal collocation on finite elements [32–34]. The set of discretized ordinary differential equations was solved with the Adams–Moulton method, implemented in the VODE procedure [35]. The relative and absolute errors of the numerical calculations were 1×10^{-6} and 1×10^{-8}, respectively.

3. Experimental

3.1. Chemicals

The only mobile phase used in this work, whether for the determination of the adsorption isotherms data, for the elution of perturbation peaks and of large size bands was a mixture of HPLC-grade methanol–water (65:35, v/v), both purchased from Fisher Scientific (Fair Lawn, NJ, USA). The solvents used to prepare the mobile phase were filtered before use on an SFCA filter membrane, 0.2 μm pore size (Suwannee, GA, USA). Uracil and butylbenzoate were both obtained from Aldrich (Milwaukee, WI, USA).

3.2. Materials

A Chromolith Performance RP-18e, 100×4.6 mm, column was used. This C_{18}-bonded, endcapped monolithic column (column 22, Merck, Darmstadt, Germany) was one of the lot of six columns used by Kele and Guiochon [14] (columns 19 to 24) for their study of the reproducibility of the properties of these columns, by Al-Bokari et al. [36] (columns 19 to 24) for the determination of the internal and external porosities of monolithic columns, by Cavazzini et al. [16] (column 24) to investigate the adsorption data of butylbenzene, and by Gritti et al. [15] (column 23) who also measured adsorption data of a few low-molecular mass compounds.

The hold-up time of this column was determined from the retention time of uracil injections. For a mobile phase composition 65:35 (v/v), the elution time of uracil is similar to that of methanol or sodium nitrate and gives an excellent estimate of the column void volume. The mean of at least five consecutive readings, agreeing to within 1%, was taken for each plateau concentration of the mobile phase (see Table 1).

The physico-chemical properties of the column supplied by the manufacturer are listed in Table 2. The external porosity of the column was obtained from Ref. [36] ($\varepsilon_e = 0.71$).

3.3. Apparatus

The data were acquired using a Hewlett-Packard (Palo Alto, CA, USA) HP 1090 liquid chromatograph. This instrument includes a multi-solvent delivery system (tank volume, 1 dm^3 each), an auto-sampler with a 25-μl loop, a diode-array UV-detector, a column thermostat and a computer data acquisition station. Compressed nitrogen and helium bottles (National Welders, Charlotte, NC, USA) are connected to the instrument to allow the continuous operation of the pump and auto-sampler. The extra-column volumes are 0.056 min and 0.340 min as measured from the auto-sampler and the pump system, respectively. All the retention data were corrected for this contribution. All measurements were carried out at a constant temperature of 23 °C.

3.4. Frontal analysis isotherm measurements

Just prior to any isotherm determination, a calibration curve was recorded for the solute at a wavelength of 293 nm. Thirty-seven concentration points were acquired, uniformly distributed within the concentration range investigated [0 g/dm^3; 10 g/dm^3]. The nonlinear calibration data are very well fitted to a third-degree polynomial.

One pump of the HPLC instrument delivered a

Table 1
Measurement of the dead time (five successive measurements) of the monolith at equilibrium with the mobile phase. Effect of the concentration of butylbenzoate in the mobile phase

Plateau concentration (g/dm^3)	t_0(1)	t_0(2)	t_0(3)	t_0(4)	t_0(5)	t_0(average)
0.0	1.434	1.432	1.432	1.432	1.433	1.433
1.2	1.424	1.423	1.424	1.424	1.426	1.424
2.4	1.416	1.416	1.416	1.417	1.415	1.416
3.6	1.408	1.408	1.408	1.406	1.408	1.407
4.8	1.398	1.399	1.397	1.399	1.399	1.398
6.0	1.388	1.389	1.390	1.389	1.391	1.390
7.2	1.382	1.381	1.382	1.381	1.378	1.381
8.4	1.370	1.374	1.374	1.373	1.372	1.373
9.6	1.361	1.362	1.363	1.360	1.362	1.362
10.8	1.348	1.350	1.350	1.352	1.351	1.350
12.0	1.333	1.334	1.334	1.331	1.332	1.333

stream of the pure mobile phase, the second pump a stream of pure sample solution. The desired concentration of the studied compound is obtained by selecting the concentration of the mother sample solution and the flow-rate fractions delivered by the two pumps. The breakthrough curves are recorded successively at a flow-rate of 1 cm^3/min, with a sufficiently long time delay between each breakthrough curve to allow enough time for the reequilibration of the column with the pure mobile phase. The injection time of the sample depends on the time required to reach the plateau concentration at the outlet of the column.

The retention volume of small pulses of uracil was determined from the average of five successive injections made at different plateau concentrations, from 0 to 12 g/dm^3, by step of 1.2 g/dm^3. The overloaded profiles needed for the validation of the fitted isotherms were recorded during the frontal analysis experiments.

Table 2
Physico-chemical properties of the monolithic silica columns supplied by the manufacturers (Merck)

Monolithic column (Merck)	
Skeleton size	1.3–1.5 μm
Macropore size	2 μm
Mesopore size	130 Å
Surface area (before C_{18} bonding)	300 m^2/g
Surface coverage (C_{18})	3.6 $\mu mol/m^2$
Total porosity	>0.80
Total carbon	19.5%
Endcapping	Yes

3.5. Perturbation chromatography measurements

The goal of this work was to provide accurate Van Deemter curves for various plateau concentrations of butylbenzoate. Hence, measurements were made at constant plateau concentration, the mobile phase linear velocity u being increased step-wise. The flow-rate sequence (24 velocities) used for each plateau was as follows:

$0.1 \rightarrow 0.15 \rightarrow 0.2 \rightarrow 0.3 \rightarrow 0.4 \rightarrow 0.5 \rightarrow 0.6 \rightarrow 0.7 \rightarrow 0.8 \rightarrow 0.9 \rightarrow 1.0 \rightarrow 1.1 \rightarrow 1.2 \rightarrow 1.3 \rightarrow 1.4 \rightarrow 1.6 \rightarrow 1.8 \rightarrow 2.0 \rightarrow 2.2 \rightarrow 2.4 \rightarrow 2.6 \rightarrow 2.8 \rightarrow 3.0 \rightarrow 3.2$ (cm^3/min)

This range allowed the observation of the transition between two distinct kinetic-governed domains (diffusion controlled at low velocity, mass transfer controlled at high velocity). This method has the disadvantage of requiring large volumes of the pure mobile phase, hence the frequent, reproducible preparation of volumes of methanol–water, 65:35. Great care must be taken during the preparation of the mobile phase. Otherwise, a significant error in the measurement of the elution time of the perturbation peaks takes place for each new plateau and the isotherm data obtained by frontal analysis and perturbation methods do not match. We prepared for

each plateau 1200 cm^3 of the pure mobile phase (780 cm^3 of methanol + 420 cm^3 of water, water being always poured into methanol). The bottle was placed in an ultrasonic bath for 30 s for degassing. Then 1 dm^3 of mobile phase was prepared at the desired plateau concentration and used for the whole sequence.

In this study, eight plateau concentrations were used, 0, 1, 2, 3, 4, 6, 8 and 10 g/dm^3. Twenty-five μl of a negative then of a positive perturbation were injected. The negative pulse feed was prepared from the previous mobile phase solution, by dilution, using a 50-cm^3 volumetric glass. The positive pulse feed was prepared by adding to the same volume of the mobile phase a small amount of solute. The concentrations of these pulses depended on the sensitivity of the detector.

In order to perform correctly the perturbation method measurements and obtain peaks with profiles as close to Gaussian as possible, it is important to record the chromatograms at the highest possible signal-to-noise ratio of the detector. The optimum wavelength was found to be $\lambda = 290$ nm. The signal-to-noise ratio was about 1000 for a concentration of 10 g/dm^3. A calibration curve was determined at this wavelength (Fig. 2). However, two effects reduce the accuracy of the peak analysis at high plateau concentrations.

1. The magnitude of the noise increases with increasing concentration, from 0.06 mAU (0 g/dm^3) to 1 mAU (10 g/dm^3), hence a 16-fold decrease in sensitivity.
2. The non-linear behavior of the UV detector decreases the sensitivity. For example, a positive step of 0.5 g/cm^3 at $C = 0$ g/dm^3 and at $C = 10$ g/dm^3 correspond to responses of 130 and 30 mAU, respectively (i.e. the signal is reduced four times).

This effect is illustrated in Fig. 3 which compares the perturbation signals after injection of a positive pulse at the two extreme plateaus, 0 and 10 g/dm^3. This illustrates the limit of validity of our experiment at high concentrations, when the feed injection concentration must be significantly different from the plateau concentration. In this case, the perturbation might not be strictly linear and the peak shape might no longer be Gaussian, due to the nonlinear behavior of the isotherm. Yet, the concentration of the injected sample must be high enough so that the width and retention time of the signal can be measured with enough accuracy to determine a meaningful value of the HETP. Consequently, we had to increase pro-

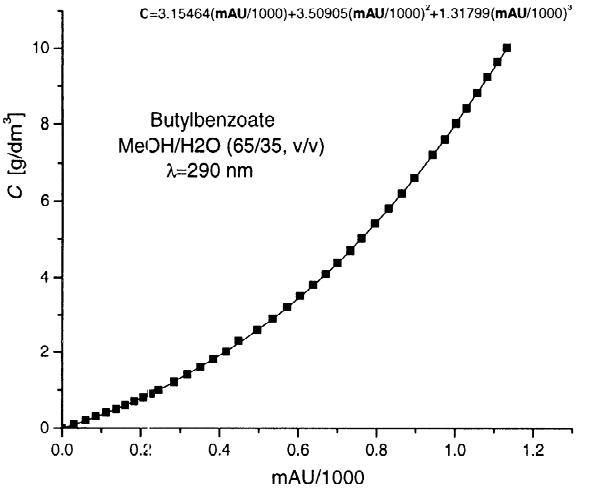

Fig. 2. Typical calibration curve obtained for butylbenzoate at $\lambda = 290$ nm. The nonlinear calibration is well fitted to a third degree polynomial. Note the higher detector sensitivity for the lowest solute concentration. $T = 295$ K.

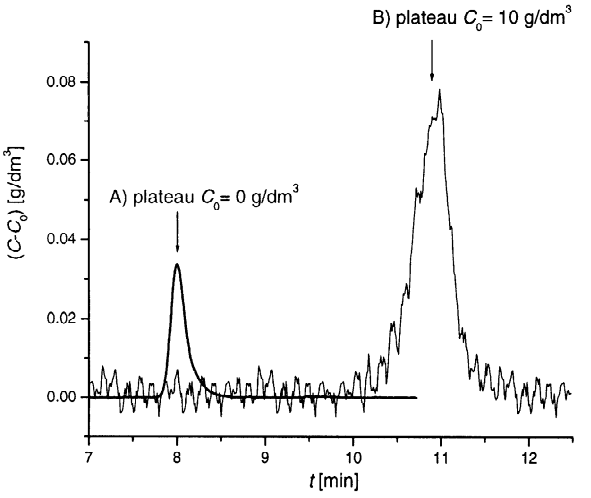

Fig. 3. Effect of the level of the plateau concentration of butylbenzoate on the detector sensitivity. Pulse injection of 25 μl of butylbenzoate. (A) $C_{inj} = 0.25$ g/dm^3 on the plateau concentration 0 g/dm^3; (B) $C_{inj} = 12$ g/dm^3 on the plateau concentration 10 g/dm^3. Methanol–water (65:35, v/v), flow-rate 1 cm^3/min, $T = 295$ K.

Table 3
Inlet concentration of the 25 μl injected solution applied in perturbation chromatography. The outlet top (positive pulse) and bottom (negative pulse) concentration of the perturbations are also given

Plateau concentration (g/dm^3)	Positive (C_+) pulse inlet concentration (g/dm^3)	Outlet top concentration (g/dm^3)	Negative (C_-) pulse inlet concentration (g/dm^3)	Outlet bottom concentration (g/dm^3)
0	0.25	0.034	–	–
1	1.25	1.027	0.75	0.974
2	2.30	2.049	1.70	1.964
3	3.30	3.031	2.70	2.973
4	4.40	4.039	3.60	3.963
6	6.90	6.093	4.20	5.813
8	9.50	8.106	6.20	7.835
10	12.00	10.055	8.00	9.910

gressively the pulse size when the plateau concentration was increasing. Table 3 reports the concentrations of the negative and positive pulses injected and the size of the perturbation recorded for a mobile phase velocity of 0.7 cm^3/min. The maximum concentration of the feed pulse decreases 10-fold on average during its elution along the column (more at the highest concentrations).

4. Results and discussion

4.1. Determination of the adsorption isotherm by frontal analysis

In a previous report [15], we showed that the adsorption data measured for butylbenzoate on the monolithic column 23 ($\varepsilon_t^0 = 0.841$), with methanol–water (65:35, v/v) as the mobile phase, fitted well to the liquid–solid extended BET model. The saturation capacity was $q_S = 209.2$ g/dm^3 and the surface equilibrium constants were $b_S = 0.120$ dm^3/g and $b_L = 0.045$ dm^3/g. Thus the Henry constant was $q_S b_S = 25.10$. In this case, we assumed that the total porosity was independent of the mobile phase concentration.

4.1.1. Variation of the total and internal porosities with the plateau concentration

The total porosity of column 22 was derived from the retention of uracil, a non-retained compound. Its retention time decreases with increasing plateau concentration, by about 7% between 0 and 12 g/dm^3. If we assume that the adsorption of butylbenzoate takes place only on the surface of the mesopores, inside the monolith skeleton, this means that the internal porosity (ε_p) of the monolith decreases according to:

$$\varepsilon_p = \frac{(\varepsilon_t - \varepsilon_e)}{(1 - \varepsilon_e)} \tag{10}$$

where the external porosity is assumed to be constant (with $\varepsilon_e = 0.71$). Fig. 4 shows the evolution of the internal porosity with increasing plateau concentration. The relative decrease of ε_p is ~40%, which is all but negligible. Assuming spherical mesopores,

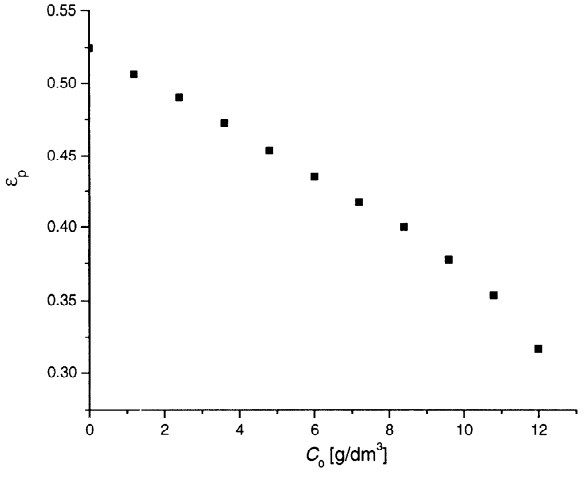

Fig. 4. Variation of the monolith skeleton particle ε_p as a function of the plateau concentration C_0. $T = 295$ K.

this means that, at the maximum mobile phase concentration used, their initial average diameter of 130 Å is reduced to $130\times(0.4)^{1/3}=96$ Å. The effect on the adsorption isotherm measurement will be considered later. This effect may also have important consequences on the mass transfer kinetics, since parameters such as the effective pore diffusivity depend directly on the internal porosity of the stationary phase. Note that, in the calculation of the amount adsorbed per unit volume of stationary phase V_a, this latter volume is the sum of the volumes of the silica and of the bonded C_{18} chains. The stationary phase volume, supposed to be constant, is the difference between the geometrical volume of the column, V_G, and the hold-up volume, V_0, at the zero plateau concentration, assuming that the adsorbate can access the whole surface area of the solid silica material (i.e. $V_a = V_G - V_0$).

4.1.2. Effect of a variable total porosity on the adsorption isotherm measurement

The breakthrough curves recorded at 1 cm^3/min are shown in Fig. 5 for plateau concentrations varying from 0.4 to 9.6 g/dm^3. They are in excellent agreement with those obtained earlier on column 23 [15], exhibiting a front shock layer at low concentrations and a diffuse front boundary at high concentrations. This effect is especially important for the highest concentration steps. Using the method of equal area to determine the amount adsorbed (see Eqs. (1) and (2)), we determined the adsorption isotherm at 295 K (not shown, see Ref. [15]).

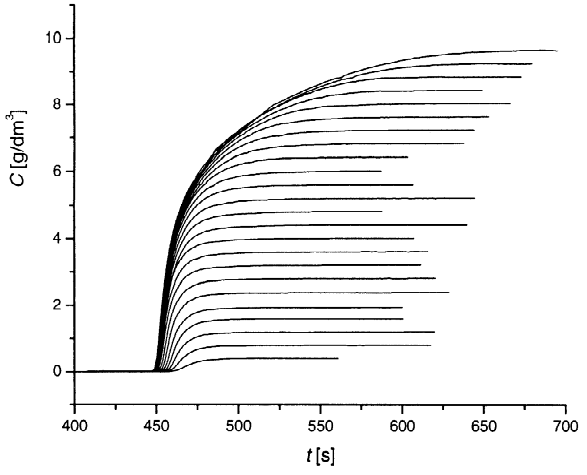

Fig. 5. Experimental front parts of the breakthrough curves of butylbenzoate with methanol–water (65:35, v/v) and the C_{18} bonded monolith column as the mobile and stationary phase, respectively. Application of a concentration step of 0.4 g/dm^3 from $C_0=0.4$ to $C_0=9.6$ g/dm^3. $T=295$ K.

If we assume that the total porosity remains constant, an excellent fit of the data to the BET model is obtained . The best parameters for q_S, b_S and b_L are 286.8 g/dm^3, 0.0990 dm^3/g and 0.0393 dm^3/g, respectively. The Henry constant is thus 28.4. These values differ slightly from those obtained with the monolithic column 23 but are consistent. They confirm the similarity between the equilibrium constants obtained with a column packed with C_{18} silica particles and with a monolithic column when the surface chemistries are equivalent, whatever the mobile phase composition [15]. With the same mobile phase composition (methanol–water, 65:35, v/v) the equilibrium constants on the packed column were $b_S=0.098$ g/dm^3 and $b_L=0.0396$ g/dm^3. Table 4 summarizes the variation of the coefficients of the BET model for columns 22 and 23. There is no clear explanation for the difference between the saturation capacities of columns 22 and 23 at 65:35. However, the data for the monolithic column 22 and the packed column are most consistent.

We showed earlier that the hold-up time decreases with increasing mobile phase concentration. Eq. (2) accounts for the influence of this phenomenon on the amount adsorbed. Let us assume that the change of the void volume $V(C)$ is due to the increase of the volume occupied by the layers of butylbenzoate adsorbed on the surface. The void volume at concentration C becomes:

$$V_0(C) = V_0(0) - \frac{q^*(C)V_{col}(1-\varepsilon_t^0)}{\rho_S} \qquad (11)$$

where ρ_S is the density of butylbenzoate adsorbed on the adsorbent surface. The experimental values of $V_0(C)$ in the whole concentration range were fitted to Eq. (11), assuming the previous set of coefficients for $q^*(C)$ ($q_S=286.8$ g/dm^3, $b_S=0.09901$ dm^3/g, $b_L=0.03931$ dm^3/g), the measured dead volume at the zero plateau concentration $V_0(0)=1.4327\times10^{-3}$ dm^3, the actual column volume $V_{col}=1.6619\times10^{-3}$ dm^3, hence a total porosity $\varepsilon_t^0=0.8621$. As a consequence, the only adjustable parameter was the

Table 4
Best BET isotherm parameters obtained on the monolith column (no. 22). Comparison with previous adsorption data on the monolith column (no. 23) and a packed C_{18} column (Waters) [15]

Mobile phase methanol–water (v/v)	Column	Fisher	q_S (g/dm^3)	IC_{95} (%)	b_S (dm^3/g)	IC_{95} (%)	b_L (dm^3/g)	IC_{95} (%)
60:40	Monolith no. 23	3.0E+04	202.7	5.2	0.212	6.8	0.085	2.8
60:40	Packed no. 5	9.9E+04	127.1	2.9	0.211	3.8	0.085	1.6
65:35	Monolith no. 23	1.1E+05	209.2	3.9	0.120	4.7	0.0450	2.7
65:35	Monolith no. 22	6.1E+04	286.8	4.7	0.099	5.5	0.0390	3.1
65:35	Packed no. 5	2.2E+05	164.1	3.2	0.098	3.7	0.0396	2.2
70:30	Monolith no. 23	7.8E+04	203.5	8.0	0.073	8.9	0.0270	6.7
70:30	Packed no. 5	1.6E+04	129.7	5.6	0.073	6.1	0.0280	4.5

average density ρ_S of the adsorbed compound . Fig. 6 shows the result of this fit. The best fit was found for a density of 0.884, ~10% less than the density of the pure liquid compound, 1.010. This result suggests that solute–solute interactions in the stationary phase are similar to those occurring in the pure liquid compound. The lower density might be explained by the presence of the C_{18} chains amidst the first layers of adsorbed butylbenzoate molecules, causing disorder and dilution.

The best parameters of the adsorption isotherm were recalculated using the void volume corrected through Eq. (11). The new values, q_S, b_S and b_L are now 288.8 g/dm^3, 0.0983 dm^3/g and 0.03961 dm^3/g, respectively. They differ from the former ones by less than 1.1%. For illustration, Fig. 7 shows the plots of the two sets of q^*/C versus C indicating the small degree to which the slope of the chord of the isotherm is underestimated. The influence of the variation of the porosity with the concentration can be neglected.

4.1.3. Validation of the adsorption isotherm measurements

A first attempt at validating the equilibrium isotherm by calculating overloaded band profiles was made, using the equilibrium-dispersive model of chromatography with the first set of numerical values of the isotherm parameters (q_S=286.8 g/dm^3, b_S=

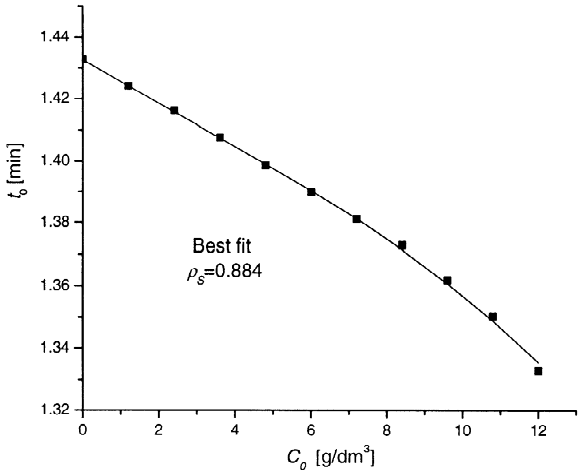

Fig. 6. Best fit of the experimental dead time points (Eq. (11)) for a plateau concentration C_0 of butylbenzoate ranged between 0 and 12 g/dm^3. Estimation of the average density of the multilayer system density ρ_S.

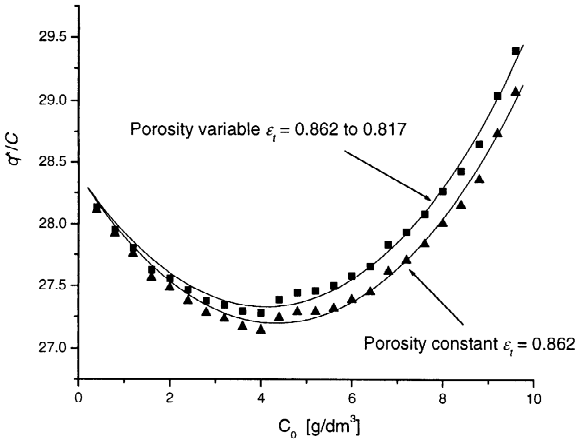

Fig. 7. Experimental isotherm (plots of q^*/C, confirming the existence of an inflection point) of butylbenzoate on the monolithic column with methanol–water (65:35, v/v) as the mobile phase assuming a constant (0.862) or the actual variable column porosity. T=295 K.

0.09901 dm^3/g, and $b_L = 0.03931$ dm^3/g). These calculations were performed using a constant value of the porosity, $\varepsilon_t = 0.8621$, obtained for the zero plateau concentration.

Three different feed concentrations and injection times were used in each case. Figs. 8–10 compare the calculated and experimental results. In each case, the column efficiency was chosen in order to obtain nearly the same peak height for the two profiles. The general agreement between experimental and calculated profiles is good and the differences suggest that they are due to incorrect estimates of the mass transfer kinetics, not to an isotherm model error. At the lowest concentration ($C_{inj} = 0.4$ g/dm^3, Fig. 8), the best BET isotherm slightly overestimates the retention times, by $\sim +1.2\%$. At the intermediate concentration ($C_{inj} = 4.4$ g/dm^3, Fig. 9), the agreement between the experimental and simulated profiles is best, especially for the two large injection times. At the highest concentration ($C_{inj} = 9.2$ g/dm^3, Fig. 10), it was not possible to achieve a good agreement for the front of the profiles. This is explained by the need to assume a constant column efficiency for profiles calculated with the ED model. Note that the best value of the column efficiency decreases with increasing sample size, hence concentration. These results suggest that the mass transfer kinetics depends on the concentration of solute. To elucidate this effect, we measured the column efficiency at different plateau concentrations, using perturbation chromatography (see Experimental).

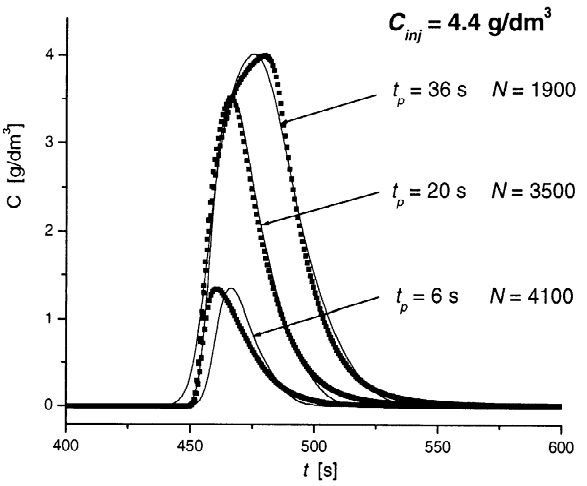

Fig. 9. Comparison between calculated (dashed line) and experimental (dotted line) band profiles. Injection of a solution of butylbenzoate at 4.4 g/dm^3 for different injection time (t_p). ED model. The efficiency N is obtained for equivalent peak height between the two curves. Monolith column, methanol–water (65:35, v/v), flow-rate 1 cm^3/min, $T = 295$ K.

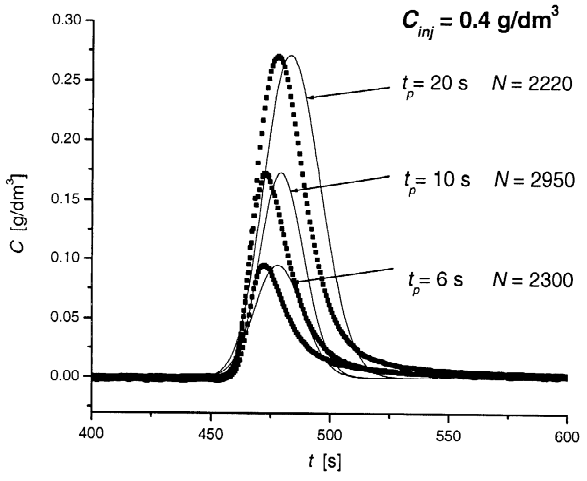

Fig. 8. Comparison between calculated (dashed line) and experimental (dotted line) band profiles. Injection of a solution of butylbenzoate at 0.4 g/dm^3 for different injection times (t_p). ED model. The efficiency N is obtained for equivalent peak height between the two curves. Monolith column, methanol–water (65:35, v/v), flow-rate 1 cm^3/min, $T = 295$ K.

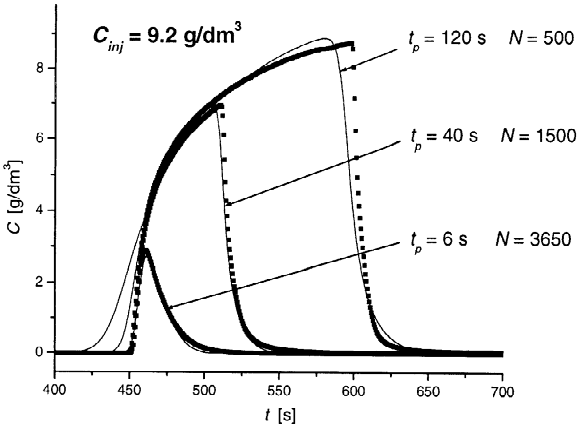

Fig. 10. Comparison between calculated (dashed line) and experimental (dotted line) band profiles. Injection of a solution of butylbenzoate at 9.2 g/dm^3 for different injection time (t_p). ED model. The efficiency N is obtained for equivalent peak height between the two curves. Monolith column, methanol–water (65:35, v/v), flow-rate 1 cm^3/min, $T = 295$ K.

4.2. Determination of the HETP of the monolithic column by perturbation chromatography

The perturbation method was first validated by comparing the adsorption data obtained by this method and those derived from frontal analysis.

4.2.1. Adsorption isotherm: comparison between frontal analysis and perturbation chromatography

The retention time of the perturbation pulse is related to the adsorption data through Eq. (5). This equation gives the slope of the isotherm at the plateau concentration. Averaging the elution times of the positive and negative pulses, the isotherm slope is given by:

$$\left.\frac{\mathrm{d}q}{\mathrm{d}C}\right|_{\bar{C}} = \frac{\varepsilon_t(\bar{C})}{1-\varepsilon_t^0}\cdot\left(\frac{V}{\varepsilon_t(\bar{C})V_{col}}\cdot\frac{t_R(\bar{C}_+)+t_R(\bar{C}_-)}{2}-1\right) \quad (12)$$

Fig. 11 illustrates the results obtained. The pulses were recorded at a flow-rate of 0.7 cm^3/min for the eight plateau concentrations. The average elution time of the two pulses is linearly related to the slope of the isotherm. Thus, the results are consistent with those in Fig. 7 and with an S-shaped isotherm. From 0 g/dm^3 to ca. 4 g/dm^3, the elution time of the pulses decreases slowly with increasing concentration while, from 4 to 10 g/dm^3, it increases rapidly, the shape of the isotherm passing from concave to convex upward. As explained in the Experimental section, it was necessary to inject too large a positive or negative concentration pulse to obtain a measurable signal (see Table 3). As a consequence, especially at high concentrations, the perturbation is not linear, the peak shape is not Gaussian, and a significant error would be made if the retention times of only the positive or the negative pulses would be measured. This is illustrated in Fig. 12 by the plots of the difference between the elution times of the positive and negative pulses.

The data in Fig. 12 indicate the range of validity of the perturbation method for the derivation of accurate data regarding the mass transfer kinetics from systematic measurements of the HETP of perturbation pulses as a function of the mobile phase velocity. As can be seen in this figure, the perturbation is linear for plateau concentrations between 0 and 4 g/dm^3. Then, the variation of the retention times is in the range of the experimental noise. Beyond 4 g/dm^3, the elution time of the positive pulse is systematically larger than that of the negative one, the perturbation peaks are unsymmetrical

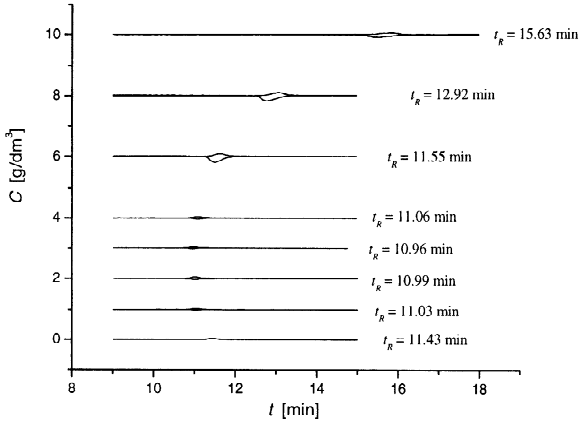

Fig. 11. Perturbation peaks recalculated according to the calibration curve in Fig. 2 at eight successive plateau concentrations C_0 of butylbenzoate (0, 1, 2, 3, 4, 6, 8, 10 g/dm^3). Note the variation of the elution time (t_R) of the impulses. Initial pulse concentrations are tabulated in Table 3. Monolith C_{18} column, methanol–water (65:35, v/v), flow-rate 0.7 cm^3/min, $T=295$ K.

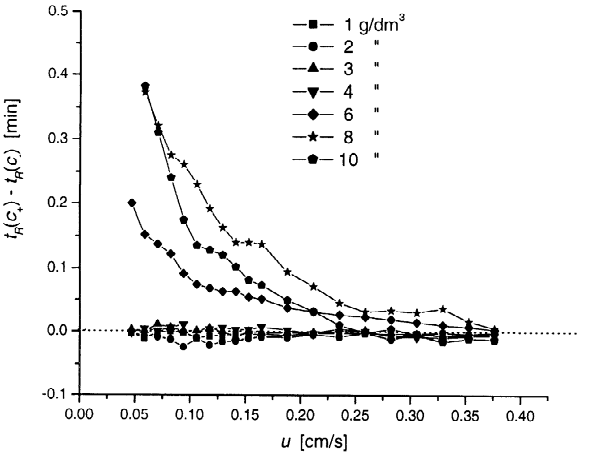

Fig. 12. Elution time difference between the positive (t_R+) and negative (t_R-) perturbation peak. Note the systematic positive difference for the three last concentration plateaus at 6, 8 and 10 g/dm^3.

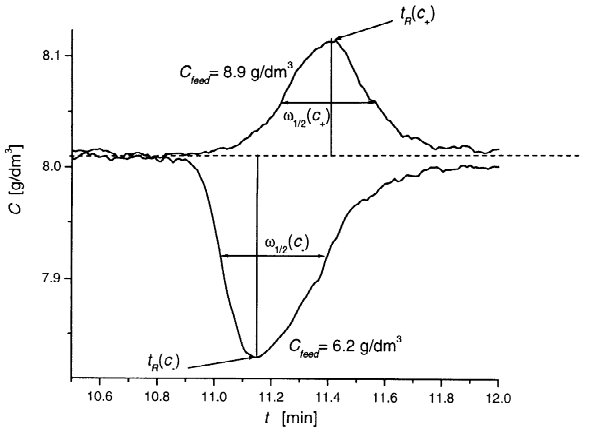

Fig. 13. Effect of thermodynamics on the recorded positive and negative impulses at the plateau concentration 8 g/dm^3. Around 8 g/dm^3, the second derivative of the BET isotherm is positive. The positive time difference observed represents about 2% of the average elution time. Note that due to the asymmetry of the peak, a correction factor is necessary to estimate a correct pure kinetic efficiency . Monolith C_{18} column, methanol–water (65:35, v/v), flow-rate 1 cm^3/min, T=295 K.

(Fig. 13), and they are too wide. Using the average time in Eq. (12) corrects for the elution time difference. However, it does not seem possible to easily correct for the increase in peak width.

Fig. 14 compares plots of the slope of the isotherm

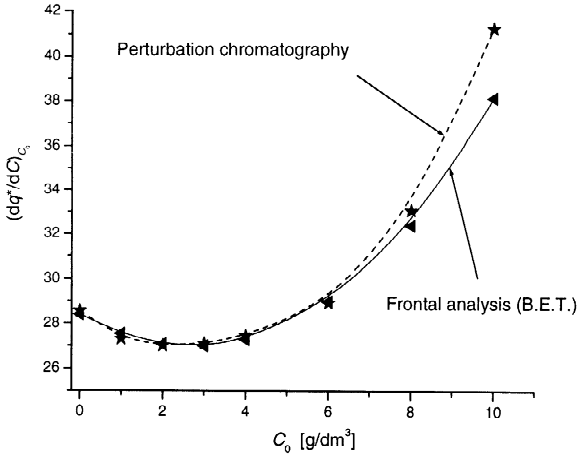

Fig. 14. Comparison between adsorption data (local slope of the isotherm) derived from perturbation chromatography and frontal analysis methods. Monolith C_{18} column, methanol–water (65:35, v/v), flow-rate 1 cm^3/min, T=295 K. (★) Perturbation chromatography, (▲) frontal analysis.

obtained by fitting the frontal analysis data to the BET isotherm model assuming a variable skeleton porosity (see Fig. 7) and the perturbation data to the first differential of the BET isotherm function (Fig. 7). For the sake of consistency, the latter data were those acquired at the flow-rate of 1 cm^3/min used in frontal analysis. An excellent agreement between the results of the two methods was obtained, except at the highest concentration (10 g/dm^3). The error in this case might stem from flow-rate errors at high solute concentrations.

4.2.2. Measurement of the local HETP using perturbation chromatography

The results of the previous section demonstrate that accurate HETP data could be derived from the perturbation peaks in the range of plateau concentrations between 0 and 4 g/dm^3. In this range, the perturbation behaves linearly and the width of its peak at half-height can be used to derive a value of the HETP of the peak, using Eq. (6), that contains essentially only the contribution of kinetic origin, H_{kin}.

On the other hand, care must be taken at plateau concentrations of 6, 8 and 10 g/dm^3 for which significant differences were found between the elution times of the positive and the negative pulse. Although the rule of additivity of the HETP contributions ($H_{ap} = H_{kin} + H_{th}$) does not apply rigorously in nonlinear chromatography [37–39], Dose and Guiochon [37] demonstrated that, at moderate values of the loading factor, the ratio N_{ap}/N_{kin} can be approximated with excellent agreement between experimental and calculated results by:

$$\frac{N_{ap}}{N_{kin}} = \frac{5.545}{N_{kin}} \cdot \frac{(2-\sqrt{L_f})^4}{(4L_f - L_f)^2} \cdot \left[1 + \frac{t_0 + t_p}{k_0' t_0} \cdot \frac{1}{(1-\sqrt{L_f})^2}\right]^2 \quad (13)$$

where N_{ap}, N_{kin}, and N_{th} are the apparent HETP and its kinetic and thermodynamic contributions, respectively, with $N_{ap} = N_{kin}N_{th}/(N_{kin} + N_{th})$. For the pulses used in this work, the loading factor is very small and the injection time is negligible compared to the hold-up time t_0. The right-hand side of Eq. (13) can

be expanded as a power series of $\sqrt{L_f}$. The thermodynamic contribution is given by:

$$N_{th} = \frac{5.545}{L_f} \cdot \left[\frac{1+k_0'}{k_0'}\right]^2 \cdot \left[1 + \left(2.5 - \frac{4k_0'}{1+k_0'}\right) \cdot \sqrt{L_f}\right] \quad (14)$$

We estimated the loading factor by:

$$L_f = \frac{|\Delta C_0| t_p \dot{V}}{q_S \bar{\varepsilon}_t V_{col}} \quad (15)$$

with $|\Delta C_0| = 2$ g/dm^3, the largest difference between pulse and plateau concentrations, $\dot{V}t_p = 25$ μl (the volume of the pulse injections), $q_S = 250$ g/dm^3 (the saturation capacity of a column monolayer), $\bar{\varepsilon}_t V_{col} = 1400$ μl (the average void volume) and $\bar{k}_0' = 7$ (the average retention factor of butylbenzoate). We obtain a loading factor less than 0.02% and a thermodynamic efficiency contribution of about 36 000. The ratio of the apparent to the pure kinetic efficiency is given by:

$$\frac{N_{ap}}{N_{kin}} = \frac{1}{1 + \frac{N_{kin}}{N_{th}}} \quad (16)$$

If we assume that $N_{kin} < 12\,000$ plates, which is the maximum efficiency obtained for the pulses recorded under linear conditions, the relative contribution of the non-linear behavior of the isotherm to the apparent efficiency would be less than 25%. However, we cannot calculate a precise enough estimate of this correction to apply it. We can only keep in mind that our measurements of HETP overestimate it by less than 25%.

4.2.3. Analysis of the HETP curves

The HETP results are summarized in two figures. Fig. 15 shows the results obtained for the plateau concentrations of 0, 1, 2, and 3 g/dm^3, i.e. under linear conditions. The four curves are very similar and cannot be differentiated due to the experimental errors. Fig. 16 shows the results obtained at plateau concentrations of 0, 4, 6, 8 and 10 g/dm^3. In this case, significant differences are observed from one Van Deemter curve to the next.

We account for these HETP curves with the classical random-walk model of Giddings [1,28]. Although this model does not fully account for the complexities of band migration along a chromatographic bed, it has the advantage of affording simple approximations of the most important properties of the actual migration process: ‘‘the random-walk

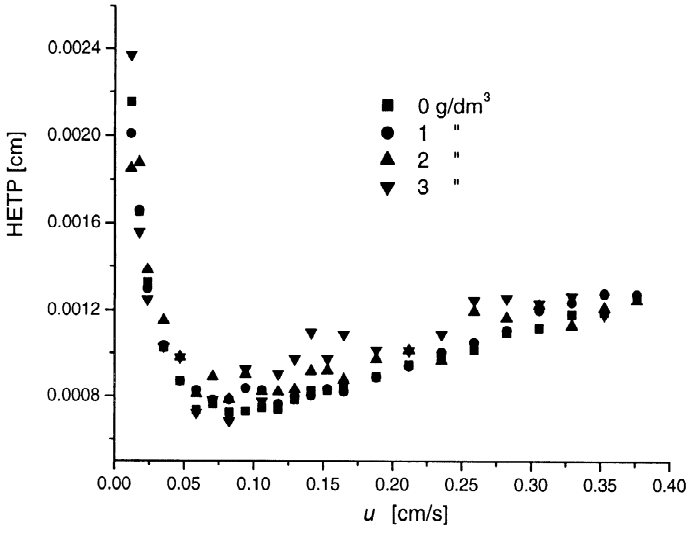

Fig. 15. Experimental HETP derived from perturbation peaks for the lowest plateau concentrations C_0 (0, 1, 2 and 3 g/dm^3). Note the similarity of the curves.

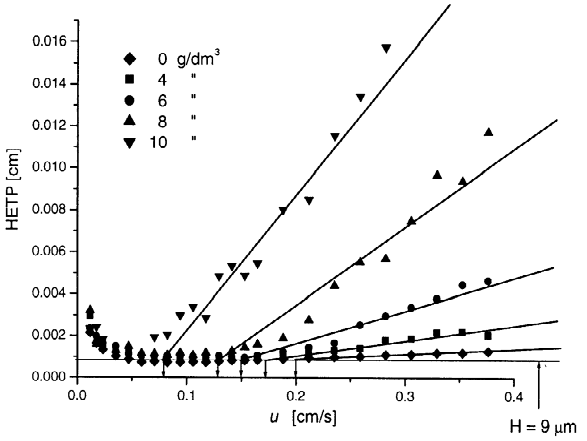

Fig. 16. Experimental HETP derived from perturbation peaks for different plateau concentrations C_0 (0, 4, 6, 8 and 10 g/dm^3). Note, this time, the sudden increase of the HETP for the highest concentrations.

model describes the essence of chromatographic zone spreading'' [1]. This is important for a first detailed investigation of the kinetics of mass transfer in a monolithic bed.

The random-walk model assumes that the different statistical molecular processes are independent of each other. The processes relevant to zone spreading are as follows.

1. The longitudinal molecular diffusion due to Brownian motion in the mobile phase. The HETP contribution is H_1:

$$H_1 = \frac{2\gamma D_m}{\bar{u}} \tag{17}$$

where γ is the tortuosity factor, slightly lower than 1, that takes into account the tortuosity and constriction of the stream-paths. D_m is the molecular diffusion coefficient and $\bar{u}$ the average linear velocity (L/t_o) of the solute in the mobile phase.

2. Eddy and radial diffusion in the mobile phase due to the irregularity of the bed structure that gives rise to frequent changes in the local direction and intensity of the velocity. Molecules travel faster in some channels than in others. Eddy and radial diffusion are two different mechanisms that allow molecules to be removed from a velocity bias. They are not independent. Giddings' coupling equation explains how these phenomena interact

$$H_2 = \frac{1}{1/H_f + 1/H_d} = \frac{1}{\dfrac{1}{2\omega_f d} + \dfrac{D_m}{\omega_d d^2 \bar{u}}} \tag{18}$$

In this equation d is the characteristic structural distance of the bed structure. For example, in packed beds, d is equal to the particle diameter d_p because all distances in the column vary in proportion to d_p. The parameters ω_f and ω_d are constants, related to the flow and the diffusion mechanism, respectively. Their magnitudes depend on the exchange process between velocity extremes in the mobile phase. Eq. (18) assumes that there is only one such exchange process to control eddy and radial diffusion in the mobile phase stream. A more complete analysis expresses the contribution of this effect as the sum of several terms similar to the one in Eq. (18). If we neglect the wall effects and the long-scaled heterogeneity of the monolith silica structure, the two main exchange processes are trans-channel and short-range inter-channel exchanges [1]. In both cases, the constant ω_f is close to 0.5. The coefficient ω_d is about 50 times lower for a trans- than for an inter-channel process (0.01 and 0.5, respectively).

3. The overall mass transfer of the solute between the stream of mobile phase and the solid-phase. This contribution lumps together the film mass transfer resistance (from the through-macropore to the mesopores in the silica skeleton), the pore diffusion inside the mesopores and the adsorption–desorption kinetics. Its contribution to the total HETP is proportional to the average linear velocity:

$$H_3 = C_S \bar{u} \tag{19}$$

If we assume no obstruction in the case of the monolithic column ($\gamma = 1$), and $\omega_f = 0.5$, the total HETP can thus be written as:

$$\text{HETP} = \frac{2D_m}{\bar{u}} + \frac{1}{\dfrac{1}{d} + \dfrac{D_m}{\omega_d d^2 \bar{u}}} + C_S \bar{u} \tag{20}$$

This equation uses only four parameters, the molecular diffusion coefficient D_m of the solute in the mobile phase, a characteristic length d of the

monolithic structure, the constant ω_d and the solid–liquid mass transfer coefficient, C_S.

4.2.3.1. Determination of the axial dispersion in the monolithic column

The Van Deemter curves shown in Fig. 15 were fitted to the model described in Eq. (20). The results are summarized in Table 5. The contributions of the three terms of the total HETP equation are schematized in Fig. 17. The very large value of ω_d means that the corresponding contribution is negligible. Eddy diffusion only is important. In this case, Eq. (20) simplifies to:

$$\text{HETP} = \frac{2D_m}{\bar{u}} + d + C_S\bar{u} = \frac{2D_L}{\bar{u}} + C_S\bar{u} \qquad (21)$$

where D_L has the general form of a dispersion coefficient [24]

$$D_L = D_m + 0.5d\bar{u} \qquad (22)$$

As expected, no significant variation of the three coefficients with increasing concentration was observed below 4 g/dm^3. In this range of plateau concentrations, we derive the following average values for the parameters: $D_m = 1.03\times10^{-5}$ cm^2/s; $d = 3.7$ μm; $C_S = 2.4\times10^{-3}$ s.

These values make physical sense. Firstly, D_m is of the same order of magnitude as the molecular diffusivity in liquids (1×10^{-5} cm^2/s). The estimate of D_m provided by the Wilke and Chang equation [40] is $\sim5\times10^{-6}$ cm^2/s [15]. Secondly, the mass transfer coefficient C_S, the slope of asymptote of the van Deemter curve, is relatively small compared to the value obtained for packed columns. For example, it is seven times lower than the value found by Miyabe and Guiochon [41] on a C_{18} packed column (particle diameter 12 μm) with *p-tert.*-butylphenol (in methanol–water mobile phase, 50:50, v/v). This shows how much the average path length in the solid particles influences C_S [6]. As a comparison, Minakuchi et al. [7] studied a similar monolith (average skeleton and through-macropores sizes of 1.5 μm and 2.2 μm, respectively) and found a C_S

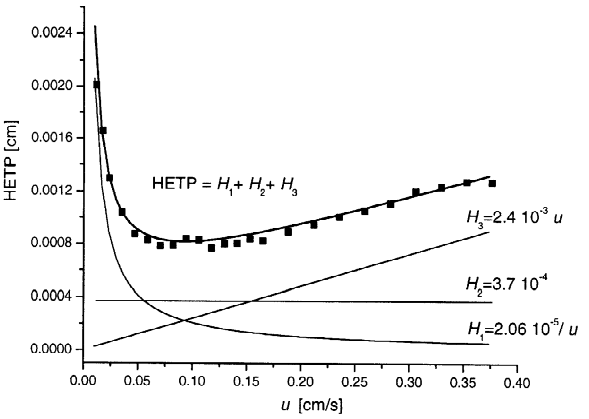

Fig. 17. Contribution of longitudinal diffusion, eddy diffusion and solid mass transfer resistance on the HETP measured on the monolithic column for the lowest plateau concentrations using Giddings' model (see text). Parameters: $D_m = 1.03\times10^{-5}$ cm^2/s, $d = 3.7$ mm, $C_S = 2.4\times10^{-3}$ s. (■) Experimental HETP on the plateau concentration $C_0 = 1$ g/dm^3.

Table 5
Best fitting parameters (D_m, d, ω_d and $C_{S,1}$) of the Giddings' HETP model (see text) as a function of the plateau concentration. Estimation of the overall solid mass transfer coefficient with the slope of the linear part of the HETP curve beyond the velocity $u_{threshold}$

Plateau C_0 (g/l)	D_m ($\times10^6$) (cm^2/s)	d (μm)	ω_d (–)	$C_{S,1}$ ($\times10^3$) (s)	r^2	$u_{threshold}$ (cm/s)	$C_{S,2}$ ($\times10^3$) (s)
0	11.09	2.84	6.5×10^{13}	2.51	0.99	0.20	1.93
1	10.13	3.50	-1.0×10^{14}	2.40	0.98	0.20	2.17
2	9.14	4.95	-4.9×10^{13}	1.94	0.89	0.20	2.20
3	10.86	3.61	1.4×10^{15}	2.70	0.91	0.20	2.31
4	(10.30)[a]	(3.70)[a]	(∞)[a]	4.20	0.81	0.17	5.63
6	(10.30)[a]	(3.70)[a]	(∞)[a]	8.33	0.75	0.15	11.7 (−25%)[b]
8	(10.30)[a]	(3.70)[a]	(∞)[a]	20.0	0.73	0.13	28.4 (−25%)[b]
10	(10.30)[a]	(3.70)[a]	(∞)[a]	41.2	0.83	0.08	42.3 (−25%)[b]

[a] The value between parentheses was kept constant during the fitting.
[b] Correction (−25%) due to thermodynamic effect on the shape of the perturbation peaks.

value of about 1.6×10^{-3} s for amylbenzene in methanol–water (80:20, v/v).

Finally, the average characteristic distance d of the chromatographic monolithic bed appears to be comparable to the domain size of the monolith defined as the sum of the average through-macropore length and the average poron (or skeleton element) size. The Performance Chromolith column of Merck has an average macropore size of 2 μm and an average skeleton size ranging between 1.3 and 1.6 μm. The best d value describes well the characteristic length of the monolith column, much as the particle diameter does for packed columns. This result does not contradict the assumption of a constant value of ω_f, equal to 0.5 and that the velocity bias in the mobile phase is due to trans-channel and/or short-range inter-channel exchange processes caused by the flow mechanism. However, no experimental data are available regarding the actual flow velocity distribution in porous monoliths. This kind of information would be useful to confirm our results.

4.2.3.2. Determination of the skeleton/through-macropores mass transfer coefficients

We consider now the Van Deemter plots obtained at high plateau concentrations (see Fig. 16). At low linear mobile phase velocities (between 0.01 and 0.1 cm/s) the curves are quite similar to those acquired at low concentrations, especially since we know that the values of the HETP obtained for the plateau concentrations of 6, 8 and 10 g/dm^3 are overestimated (see the previous section). In this velocity range, the column efficiency is controlled by axial dispersion (D_L) while the mass transfer resistance between the solid skeleton and the flow mobile phase has little influence. At higher concentration, the HETP increases with increasing mass transfer resistance and with increasing velocity. The results in Table 5 and Fig. 16 show that the high concentration experimental data fit poorly to Eq. (21) if we assume that the molecular diffusivity D_m (1.03×10^{-5} cm^2/s) and the eddy diffusion length d (3.7 μm) are constant. The regression coefficients between 0.75 and 0.80 show that Eq. (21) does not account properly for the experimental profiles and particularly for their wide minimum region. It is a typical property of monoliths to provide good column efficiencies even at high velocities and the low value of C_S accounts for this phenomenon. The data in Fig. 16, however, suggest that the contribution of the mass transfer resistance increases at high concentration, i.e. that C_S increases with increasing concentration. Indeed, the values reported in Table 5 increase steadily from the lowest concentration ($C_{S,1}=0.0024$ s) to 10 g/dm^3 ($C_{S,1}=0.0410$ s). This result is confirmed by Fig. 18 in which the theoretical and experimental values of C_S and its contributions are compared. A more sophisticated model of the mass transfer contribution is needed.

In the general rate model of chromatography, the mass transfer coefficient C_S is related to three main kinetic phenomena, the film mass transfer, or transfer between the mobile phase stream and the internal pores (i.e. from the through-macropores to the porons in monoliths), diffusion in the internal pores of the skeleton, and adsorption–desorption. The kinetics of these contributions are controlled by the film mass transfer coefficient, the effective pore diffusion coefficient D_{eff}, and the adsorption–desorption constant of the solute. In locally linear chromatography, the contributions of these three effects are additive. Miyabe and Guiochon [42] derived a physical model of the monolith, assuming an assembly of elementary cylinder-shape pieces for the skeleton, surrounded by a coaxial volume available for the stream of mobile phase. Using moment

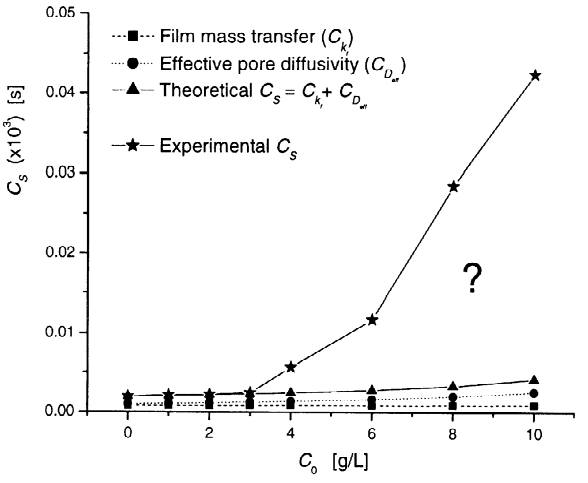

Fig. 18. Comparison between experimental and estimated overall mass transfer coefficient assuming the contributions of film mass transfer and pore diffusivity kinetics as a function of the plateau concentration.

analysis, they derived the following general expression for the HETP. It is similar to the one used for spherical particles. If we assume a fast adsorption–desorption process on the solid surface, the overall mass transfer coefficient C_S is given by:

$$C_S = 2\left(\frac{K}{1+K}\right)^2 \cdot \left[\frac{d_S}{4Fk_f} + \frac{d_S^2}{32FD_{eff}}\right] \quad (23)$$

In this equation, the numerical coefficients 4 and 32 replace the classical values of 6 and 60, respectively, obtained for spherical particles. F is the external phase ratio $(1-\varepsilon_e)/\varepsilon_e$. The locally linear equilibrium constant K is given by:

$$K = F\left(\varepsilon_p + (1-\varepsilon_p)\frac{dq}{dC}\bigg|_{\bar{C}}\right) \quad (24)$$

It depends on the skeleton porosity ε_p and on the local slope of the isotherm. The skeleton or internal porosity is calculated by combining Eqs. (10) and (11) ($\varepsilon_t = V_0(C)/V_{col}$). d_S is the average diameter of the skeleton cylinders. The mass transfer coefficient k_f depends usually on the mobile phase velocity u. In liquid phase, it may be correlated to u using the Wilson and Geankoplis correlation [43]:

$$Sh = \frac{k_f d_S}{D_m} = \frac{1.09}{\varepsilon_e}\cdot\left(\frac{\bar{u}d_S}{D_m}\right)^{0.33}$$
$$\text{or } k_f = \frac{1.09}{\varepsilon_e}\cdot\left(\frac{\bar{u}D_m^2}{d_S^2}\right)^{0.33} \quad (25)$$

In the present case, the average skeleton size d_S is 1.4×10^{-4} cm, the external porosity ε_e is 0.71, hence F is 0.408, the molecular diffusion coefficient D_m is $\sim10^{-5}$ cm^2/s (see earlier, experimental results). The local slope of the isotherm is calculated from the derivative of Eq. (7), with the best set of parameters obtained ($q_S = 288.8$ g/dm^3, $b_S = 0.09834$ dm^3/g, $b_L = 0.03961$ dm^3/g):

$$\frac{dq}{dc}\bigg|_{\bar{c}} = q_S b_S \cdot \frac{1 - b_L^2\bar{c}^2 + b_S b_L \bar{c}^2}{(1-b_L\bar{c})^2(1-b_L\bar{c}+b_S\bar{c})^2} \quad (26)$$

Combining the first term of Eq. (23) with Eq. (25) or (26), we derived the dependence of the contribution to the mass transfer coefficient associated with k_f as a function of the linear mobile phase velocity for the different plateau concentrations:

$$C_{k_f} = 2\left(\frac{K}{1+K}\right)^2 \cdot \frac{d_S}{4Fk_f} \quad (27)$$

The magnitude of the film transfer resistance is small. It varies between 0.6 and 1.4×10^{-3} s and is independent of the concentration of butylbenzoate (in the range from 0 to 10 g/dm^3) and of the mobile phase velocity (0.05 to 0.37 cm/s), as illustrated in Fig. 19. Hence, it cannot account for the large increase of C_S observed at high concentrations and flow velocities. On the other hand these values are in reasonably good agreement with the average mass transfer coefficient obtained for the lowest concentrations ($C_S = 2.4\times10^{-3}$ s).

In the monolith, pore diffusion takes place in the mesopores, in the stagnant mobile phase. We assume first that there is no surface diffusion of the solute on the adsorbent surface. Then, as a first approximation, D_{eff} can be estimated by the effective pore diffusivity, well described for a silica particle [44] by the equation:

$$D_{eff} = \frac{K_p \varepsilon_p}{\tau} \cdot D_m \quad (28)$$

where K_p is the hindrance parameter that accounts for the exclusion of the solute from pore regions near the pore wall (due to the finite average size, r_m, of the solute) and for the viscous drag due to friction at

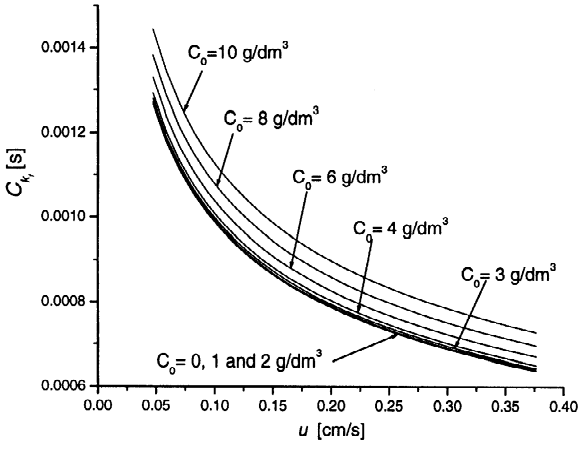

Fig. 19. Evolution of the film mass transfer coefficient C_{k_f} as a function of the linear flow velocity (assuming Wilson and Geankoplis correlation) and the plateau concentration C_0. Note the slight variation of C_{k_f} with both these variables and the small values, as well.

the pore wall. The important parameter in this equation is the ratio of the solute average radius to the average pore radius $\lambda_m = r_m/R_p$. The diameter of butylbenzoate was estimated from its structure [45]. Its length is 11.08 Å, so, we assumed $r_m = 5$ Å. As demonstrated in Section 4.1.1, the average pore diameter is not constant and can be estimated as follows (for $C_0 = 0$ g/dm^3, the average pore diameter is $R_p^0 = 65$ Å and the initial skeleton porosity is $\varepsilon_p^0 = 0.525$):

$$R_p = \left(\frac{\varepsilon_p}{\varepsilon_p^0}\right)^{1/3} \cdot R_p^0 = 80.6\varepsilon_p^{1/3}\ (\text{Å}) \text{ and } \lambda_m = \frac{0.062}{\varepsilon_p^{1/3}} \quad (29)$$

The lowest value measured for ε_p is about 0.36. Thus λ_m will never exceed 0.20 and we can use the correlation of Brenner and Gaydos [46] to estimate the hindrance parameter:

$$K_p = \frac{1 + 9/8\ \lambda_m \ln \lambda_m - 1.593\lambda_m}{(1-\lambda_m)^2} \quad (30)$$

In Eq. (28), τ is the tortuosity factor (>1) that represents the effective average length of the pores in the silica skeleton. We estimated it using the Wakao and Smith correlation [47]:

$$\tau = \frac{1}{\varepsilon_p} \quad (31)$$

Finally, it is possible to formulate D_{eff} as a function of the skeleton porosity and the molecular diffusion coefficient D_m:

$$D_{eff} = D_m \varepsilon_p^2 \cdot \left(\frac{1 + \frac{0.070}{\varepsilon_p^{1/3}} \cdot \ln\left(\frac{0.062}{\varepsilon_p^{1/3}}\right) - \frac{0.099}{\varepsilon_p^{1/3}}}{\left(1 - \frac{0.062}{\varepsilon_p^{1/3}}\right)^2} \right) \quad (32)$$

Combining the second term of Eq. (23) with Eq. (32), we derived the relationship between the mass transfer coefficient, the effective pore diffusivity, and the plateau concentration

$$C_{D_{eff}} = 2\left(\frac{K}{1+K}\right)^2 \cdot \frac{d_S^2}{32FD_{eff}(\varepsilon_p, D_m)} \quad (33)$$

Fig. 18 summarizes the contributions of C_{k_f} and $C_{D_{eff}}$ to the total mass transfer coefficient and compares the results to the experimental data. It demonstrates that the combination of the film mass transfer kinetics (the smaller contribution) and the pore diffusivity (the major contribution) accounts well for the actual mass transfer kinetics in monolithic columns for plateau concentrations of butylbenzoate below 3 g/dm^3. At higher concentrations, this approach fails to explain the rapid increase of the mass transfer resistance observed (Fig. 16). Even though we know that the HETP values are overestimated because of experimental problems arising at high concentrations, we also know that the effect observed far exceeds the systematic error made. Another source of mass transfer resistance must kick in at high concentrations, probably related to the build-up of a large number of successive layers of sorbed molecules.

5. Conclusion

The adsorption equilibrium data derived from the perturbation method are in excellent agreement with those obtained by frontal analysis. This test is sensitive because the best isotherm is described by a liquid–solid extended BET isotherm, a model that has a nearly linear behavior and because the apparent internal porosity of the monolith changes at high concentration due to the large number of adsorbed layers that are progressively built-up at the liquid–solid interface.

The perturbation method provides also kinetic data. Our results demonstrate that it can be used to derive Van Deemter curves under quasi-linear conditions. Serious difficulties arise, however, at high concentrations. It becomes difficult accurately to record well-defined, linear perturbation peaks. We showed how it is possible to minimize the errors made in the determination of the HETP at high plateau concentration, when the condition of local linear behavior of the isotherm can no longer be rigorously respected.

At low and moderate velocities, axial dispersion controls the HETP. Eddy diffusion and axial diffusion in the macropores control band dispersion. An exchange mechanism between the velocity bias of trans-channel and/or short-range inter-channel origin explains this phenomenon and justifies the high efficiency observed with monoliths.

At high velocities, our results show that the mass transfer kinetics is mainly controlled by pore diffusivity inside the porons or small-size elements of the monolith skeleton at low solute concentrations ($C_0 < 3$ g/dm^3). The film mass transfer contribution is small. At high plateau concentrations, the mass transfer resistance increases markedly. This might be, at least in part, due to the use of sample sizes that are too large for a small perturbation and exceed the quasi-linear range. Thus, the band broadening observed includes a contribution due to the nonlinear behavior of the isotherm. It may be, however, that a new source of mass transfer resistance becomes significant in this range, possibly in connection with the progressive filling of a large fraction of the internal porosity, as demanded by the equilibrium isotherm data. While the characteristic time of pore diffusivity is of the order of a few milliseconds, that of this new phenomenon would be of the order of 10 to 100 ms.

Acknowledgements

This work was supported in part by grant CHE-00-70548 of the National Science Foundation and by the cooperative agreement between the University of Tennessee and the Oak Ridge National Laboratory. We thank Karin Sinz, Karin Cabrera, Dieter Lubda (Merck KGaA, Darmstadt, Germany) and Fred Rabel (EM Science, Gibbstown, NJ, USA) for the generous gift of the columns used in this work and for fruitful discussions.

References

[1] J.C. Giddings, Unified Separation Science, Wiley, New York, 1991.
[2] P.A. Bristow, J.H. Knox, Chromatographia 10 (1977) 279.
[3] H. Poppe, J. Chromatogr. A 778 (1997) 3.
[4] H. Minakuchi, K. Nakanishi, N. Soga, N. Ishizuka, N. Tanaka, Anal. Chem. 68 (1996) 3498.
[5] H. Minakuchi, K. Nakanishi, N. Soga, N. Ishizuka, N. Tanaka, J. Chromatogr. A 762 (1997) 135.
[6] H. Minakuchi, K. Nakanishi, N. Soga, N. Ishizuka, N. Tanaka, J. Chromatogr. A 797 (1998) 121.
[7] N. Ishizuka, H. Minakuchi, K. Nakanishi, N. Soga, N. Tanaka, J. Chromatogr. A 797 (1998) 133.
[8] H. Minakuchi, K. Nakanishi, N. Soga, N. Ishizuka, N. Tanaka, J. Chromatogr. A 828 (1998) 83.
[9] N. Tanaka, H. Nagayama, H. Kobayashi, T. Ikegumi, K. Hosoya, N. Ishizuka, H. Minakuchi, K. Nakanishi, K. Cabrera, D. Lubda, J. High Resolut. Chromatogr. 23 (2000) 111.
[10] K. Cabrera, G. Wieland, D. Lubda, K. Nakanishi, N. Soga, H. Minakuchi, K.K. Unger, Trends Anal. Chem. 17 (1998) 50.
[11] K. Cabrera, D. Lubda, H.-M. Eggenweiler, H. Minakuchi, K. Nakanishi, J. High Resolut. Chromatogr. 23 (2000) 93.
[12] N. Ishizuka, H. Minakuchi, K. Nakanishi, K. Hirao, N. Tanaka, Colloids Surf. A: Physicochem. Eng. Asp. 187–188 (2001) 273.
[13] B. Bidlingmaier, K.K. Unger, N. von Doehren, J. Chromatogr. A 832 (1999) 11.
[14] M. Kele, G. Guiochon, J. Chromatogr. A 960 (2002) 19.
[15] F. Gritti, W. Piatkowski, G. Guiochon, J. Chromatogr. A, in press.
[16] A. Cavazzini, G. Bardin, K. Kaczmarski, P. Szabelski, M. Al-Bokari, G. Guiochon, J. Chromatogr. A 957 (2002) 111.
[17] D. Josic, A. Buchacher, A. Jungbauer, J. Chromatogr. B 752 (2001) 191.
[18] P. Zöllner, A. Leitner, D. Lubda, K. Cabrera, W. Lindner, Chromatographia 52 (2000) 818.
[19] G. Dear, R. Plumb, D. Mallett, Rapid. Commun. Mass Spectrom. 15 (2001) 152.
[20] K. Cabrera, D. Lubda, H.-M. Eggenweiler, H. Minakuchi, K. Nakanishi, J. Chromatogr. A 762 (1997) 135.
[21] M. Schulte, D. Lubda, A. Delp, J. Dingenen, J. High Resolut. Chromatogr. 23 (2000) 100.
[22] M. Schulte, J. Dingenen, J. Chromatogr. A 923 (2001) 17.
[23] L. Spoof, J. Meriluoto, J. Chromatogr. A 947 (2002) 237.
[24] G. Guiochon, S. Golshan-Shirazi, A.M. Katti, Fundamentals of Preparative and Nonlinear Chromatography, Academic Press, Boston, MA, 1994.
[25] D.M. Ruthven, Principles of Adsorption and Adsorption Processes, Wiley, New York, 1984.
[26] G. Zhong, P. Sajonz, G. Guiochon, Ind. Eng. Chem. (Res.) 36 (1997) 506.
[27] C.N. Reilley, G.P. Hildebrand, J.W. Ashley Jr., Anal. Chem. 34 (1962) 1198.
[28] J.C. Giddings, Dynamics of Chromatography I, Principles and Theory, Marcel Dekker, New York, 1965.
[29] S. Brunauer, P.H. Emmet, E. Teller, J. Am. Chem. Soc. 60 (1938) 309.
[30] M. Suzuki, Adsorption Engineering, Elsevier, Amsterdam, 1990.
[31] P.W. Danckwerts, Chem. Eng. Sci. 2 (1953) 1.

[32] K. Kaczmarski, M. Mazzotti, G. Storti, M. Morbidelli, Comput. Chem. Eng. 21 (1997) 641.
[33] K. Kaczmarski, Comput. Chem. Eng. 20 (1996) 49.
[34] K. Kaczmarski, D. Antos, J. Chromatogr. A 862 (1999) 1.
[35] P.N. Brown, A.C. Hindmarsh, G.D. Byrne, Procedure available from http://www.netlib.org.
[36] M. Al-Bokari, D. Cherrak, G. Guiochon, J. Chromatogr. A, in press.
[37] E.V. Dose, G. Guiochon, Anal. Chem. 62 (1990) 1723.
[38] S. Golshan-Shirazi, G. Guiochon, Anal. Chem. 61 (1989) 462.
[39] S. Golshan-Shirazi, G. Guiochon, Anal. Chem. 60 (1988) 2364.
[40] C.R. Wilke, P. Chang, AICHE J. 1 (1955) 264.
[41] K. Miyabe, G. Guiochon, J. Chromatogr. A 890 (2000) 211.
[42] K. Miyabe, G. Guiochon, J. Chromatogr. A, submitted.
[43] E.J. Wilson, C.J. Geankoplis, Ind. Eng. Chem. (Fund.) 5 (1966) 9.
[44] G. Carta, in: Preparatory Symposium, Work shop, Washington, DC, 2002.
[45] J. March, in: 4th ed, Advanced Organic Chemistry, Wiley, New York, 1992.
[46] D. Brenner, P. Gaydos, J. Colloid. Interf. Sci. 58 (1977) 312.
[47] N. Wakao, J.M. Smith, Chem. Eng. Sci. 17 (1962) 825.